JOURNAL OF MATERIALS SCIENCE **34** (1999) 749–761

Structure and properties of rapidly-solidified Al-rich Al-Mn-Si alloys

Part II *Atomized powder, its extrudate and the effect of blended-in SiC*

D. M. J. WILKES*, H. JONES
Department of Engineering Materials, University of Sheffield, Sheffield S1 3JD, UK
E-mail: k.a.burton@sheffield.ac.uk

Argon atomized Al-5 Mn-3 Si (wt %) powder has been extruded with and without 15 vol % added SiC particulate at 425 °C and characterized both as extruded and after 100 and 1000 h at 425 °C. As extruded matrix microstructure of discrete αAlMnSi particles of mean diameter 60 nm in an αAl matrix was similar to that for comparable melt-spun ribbon after 2 to 5 h at 425 °C and coarsening of αAlMnSi in 100 and 1000 h at 425 °C was also comparable. Hardness and proof strength of the matrix as extruded and their decrease on heat treatment matched predictions of a combined Orowan and Hall-Petch model as for the melt-spun condition. Initial hardness and tensile properties of the matrix were similar to those of extruded Al-Fe-V-Si with the same (∼15) vol per cent of silicide. Increment in Young's modulus of ∼30 GPa when SiC was present was similar to that for Al-Fe-V-Si/SiC MMC, while increments in strength and decrements in elongation to fracture were smaller for the Al-Mn-Si/SiC MMC. © *1999 Kluwer Academic Publishers*

1. Introduction

The development of high performance light materials that retain strength and stability at elevated temperatures is a continuing need for aerospace and automotive application [1–7]. One solution is to disperse a substantial volume fraction of a suitable hard second phase on a sufficiently fine scale throughout a light metallic matrix. This second phase can be a product of conventional age hardening (which is however subject to the effects of dissolution and coarsening when temperature is raised), can be a direct or indirect result of rapid solidification from the melt or an equivalent technique, or can be the result of external injection of the second phase in the liquid or solid states. This paper explores the second alternative as exemplified by the nanophase silicide dispersion in Allied's 8009 Al-Fe-V-Si alloy [8] which exhibits unusual thermal stability at temperatures as a high as 0.75 T_m (425 °C), limited only by transformation to embrittling needles of equilibrium $Al_{13}Fe_4$ at >0.8 T_m [9]. The corresponding stable silicide phase in the Al-Mn-Si system is an attractive alternative. Paris *et al.* [10–15] pioneered work on the Al-10 Mn-2.5 Si (wt %) composition and some derivatives [16–19] while Hawk *et al.* [20–23] explored Al-15 Mn-5 Si and, most recently, Büchler *et al.* [24] explored a range of stoichiometries centred on Al-10 Mn-2 Si. The present paper explores the potential of atomized Al-5 Mn-3 Si powder as a thermally stable matrix for reinforcement with blended-in SiC particulate. Its predecessors [25, 26] explored the evolution of microstructure in melt-spun Al-6 Mn-3 Si, Al-8 Mn-4 Si and Al-15 Mn-6 Si, while parallel work reported on the effect of variable Si-content in Al-7.5 Mn-2.7 to 9.8 Si [27].

2. Experimental

Argon atomized powder of composition Al-5.1 Mn-3.3 Si (wt %) was supplied (sub-45 μm fraction) by Alpoco Ltd. Coulter laser diffraction particle size analysis (Fig. 1) indicated the most frequent particle size as 3 μm, whereas the largest volume per cent was of particle size ∼30 μm. Canning, degassing and extrusion was carried out at DERA, Farnborough. One batch of the powder was pre-mixed in a triaxial shaker with 15 vol % of 2 to 10 μm SiC particulate before consolidation. The 5 h chamber degassing cycle involved evacuation, heating to 425 °C for 1 h followed by slow cooling, all under vacuum. Extrusion was carried out at 400 °C at a ram speed of 10 mm/min with water cooling of the extrudate as it emerged from the die. The extrusion ratio was 20 : 1 giving a final diameter of 11 mm. The product was ∼1.1 m long, the first and last 200 mm being discarded to remove the front end of the can and the pipe intrusion. Some of this material was heat treated for 100 and 1000 h at 425 °C.

Samples of as-received powder, consolidated and heat treated material were characterized by optical metallurgy, x-ray diffraction (XRD), scanning electron

* *Present Address*: Structural Materials Centre, DERA Farnborough, GU14 OLX, UK.

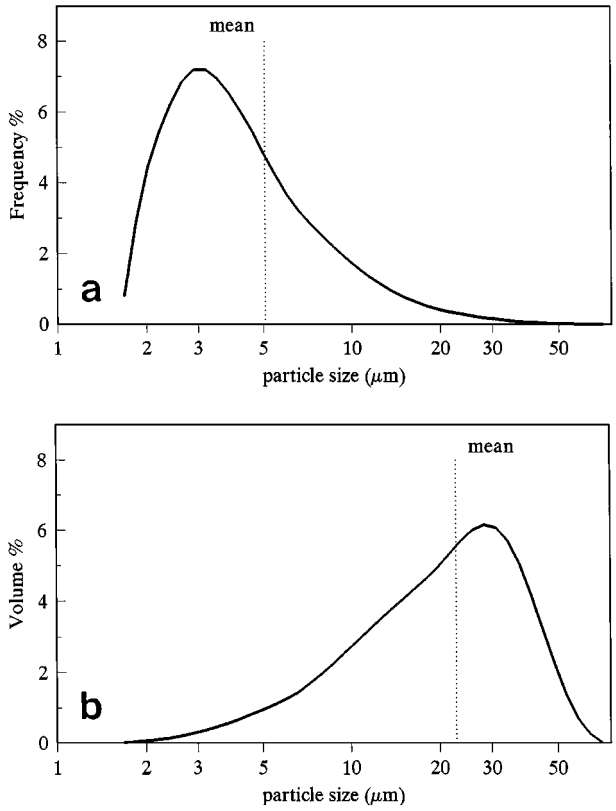

Figure 1 (a) Frequency and (b) volume particle size distribution of Al-5 Mn-3 Si atomized powder size fraction supplied by Alpoco Ltd.

microscopy (SEM) and transmission electron microscopy (TEM). XRD used CoKα radiation and SEM employed a Joel JSM 6400 microscope. TEM of atomized powder was carried out in a Phillips 400T on samples mixed with epoxy resin and forced into a copper tube of external diameter 3 mm. Slices 2 mm in thickness were ground to 200 μm and dimpled to 70 μm using a size 4 dimpling wheel with 6 μm and 1 μm diamond paste followed by Silco. Thinning to electron transparency was then achieved by ion beam milling. TEM was limited to 80 kV and a low emission setting to avoid burning off resin or heating the powder particles. TEM of extrusions was carried out on 1 mm discs sliced from the gauge length of tensile specimens. These were ground to a thickness of $\sim$100 μm and electrothinned in 25% nitric acid in methanol at below $-30\,^{\circ}$C using a current of $\sim$0.18 A and an applied voltage between 12 and 20 V depending on the solution temperature. Second phase particle sizes were measured directly from TEM negatives using a magnifying eyepiece with graticule. At least 3 foils and up to 5 different areas per foil were sampled, giving a total of at least 300 particles per condition. Vickers or Knoop microhardness measurements were made on sectioned powder particles and extrusions. Tensile tests were in accordance with BS EN 10002-1 : 1990 using a gauge length of 25 mm and a gauge diameter of 4 mm. Extension rate was initially 0.06 mm/min to determine modulus and proof stress, followed by extension at 5 mm/min until fracture occurred.

3. Results

3.1. As-atomized powder

Optical microscopy of mounted, polished and etched sections (Fig. 2) showed dendritic (zone B) structure in larger particles which became finer with decreasing particle size, with the finest particles (size <5 μm) being optically featureless (zone A) [28]. SEM of unsectioned powder (Fig. 3a, b) shows increasingly smooth surfaces and more spherical shape at decreasing particle size, with satellite smaller particles adhering to the larger particles. Backscattered electron images of sectioned powder particles (Fig. 4) indicate interdendritic segregation of Mn with increasingly fine structure down to particle sizes of 5 to 7 μm, below which nothing is resolved. TEM of the smallest particles (diameter 3 to 5 μm) showed fine cellular structure with continuous intercellular second phase (Fig. 5a) with evidence for transitions from featureless single phase αAl to two

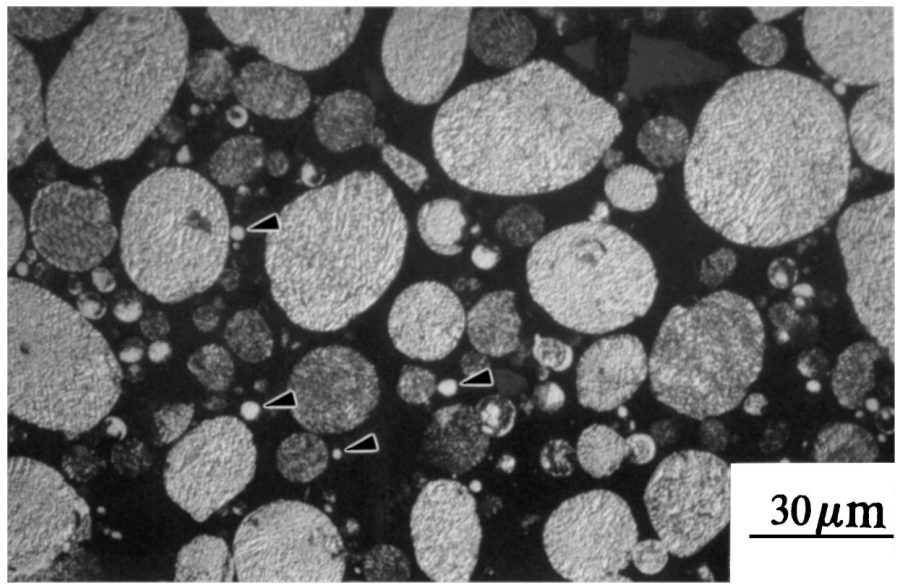

Figure 2 Optical micrograph of etched section of Al-5 Mn-3 Si atomized powder showing range of etching response from fine featureless (zone A) arrowed in smallest particles to dendritic (zone B) in larger particles.

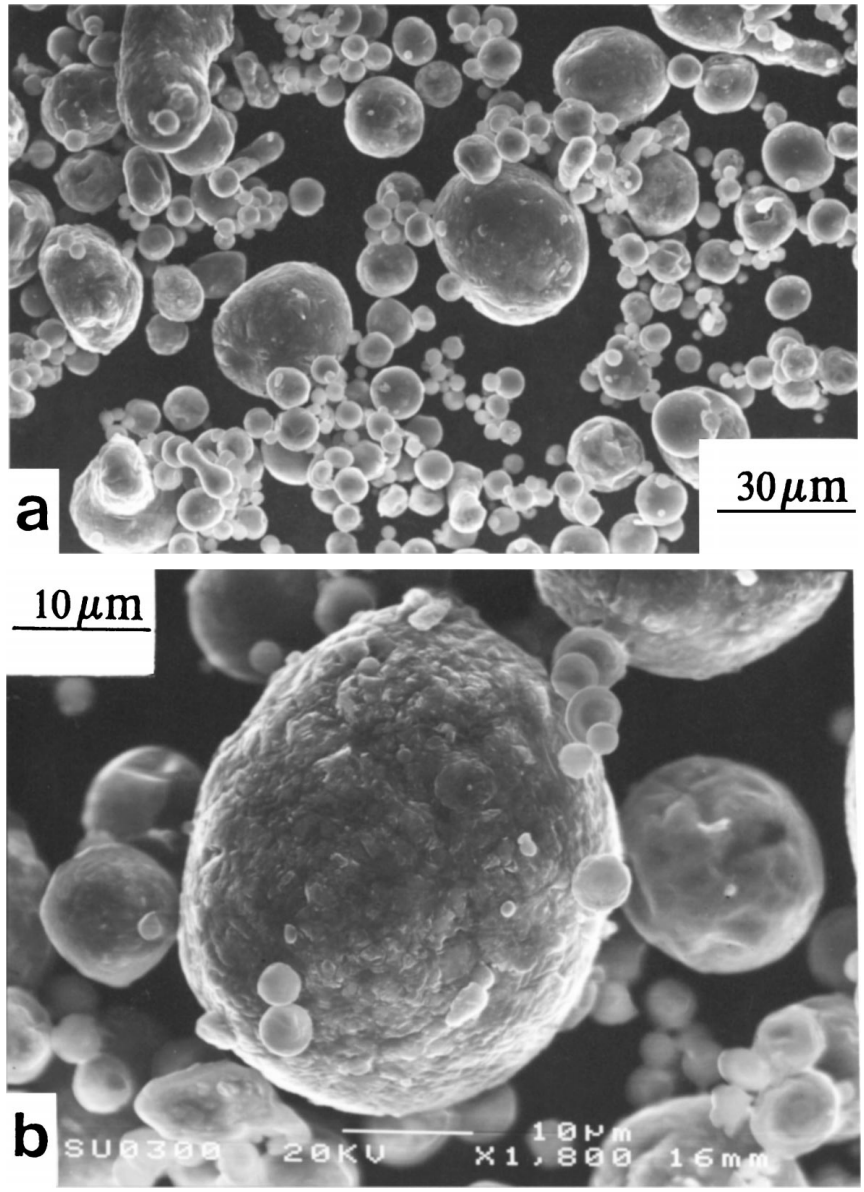

Figure 3 SEM micrographs of as-received Al-5 Mn-3 Si powder showing (a) increased sphericity and smoothness of surface with decrease in particle size and (b) smooth satellite particles adhering to rough surface of a larger particle.

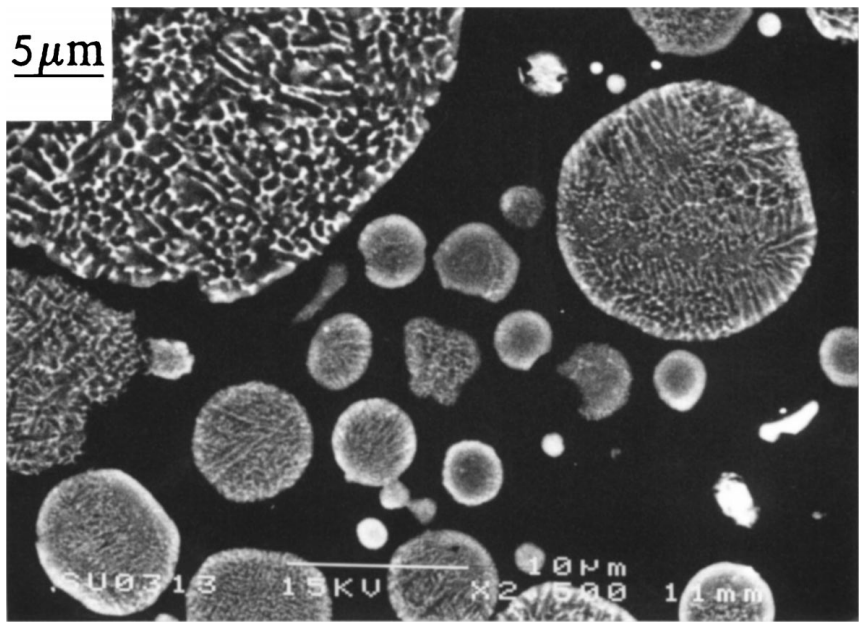

Figure 4 SEM back scattered electron micrograph from sectioned Al-5 Mn-3 Si powder particles showing segregation of Mn and reduction of scale of dendrite structure with decreasing particle size, not resolved for smallest particles.

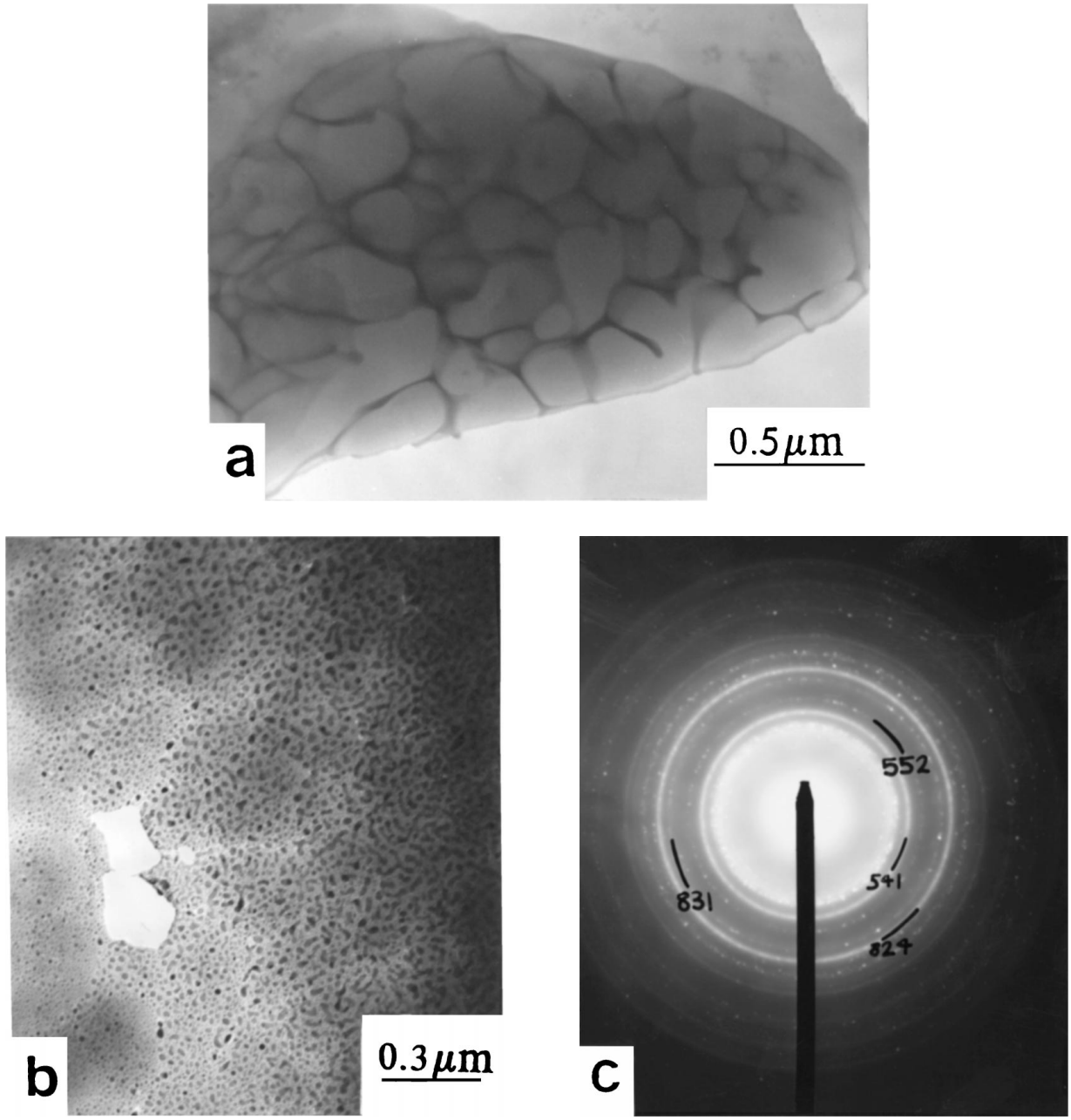

Figure 5 TEM micrographs of ion beam thinned Al-5 Mn-3 Si powder particles showing (a) cellular structure in a 3 to 5 μm particle (b) second phase precipitation in a 10 to 15 μm diameter particle (c) diffraction pattern from 20 nm particles indexed as αAlMnSi.

phase cellular structure within single particles, as reported for other systems [29, 30]. The 20 nm precipitates to the right of the perforation in the 10 to 15 μm diameter particle shown in Fig. 5b gave diffraction rings consistent with αAlMnSi (Fig. 5c). XRD data (Fig. 6) indicate αAl plus broad low intensity peaks at 48.8 and 51.8 $^\circ 2\theta$ consistent with presence of αAlMnSi as second phase at least in the larger particles which dominate the size distribution (Fig. 1b). Knoop microhardness of the larger particles was 120 ± 11 kg/mm^2.

3.2. Structure of as-extruded material

Optical microscopy of longitudinal sections (Fig. 7a, b) suggested that the microstructural variability of the as-atomized powder was retained to some extent on extrusion, with some small zone A powder particles resisting deformation quite effectively (Fig. 7b). X-ray diffraction (Fig. 6) showed all of the expected αAlMnSi peaks between 42 and 58° 2θ, and the peaks are sharper and more intense than for the as-received powder. TEM showed wide variations in size and distribution of second phase particles, ranging in size from a few nm, in regions derived from small prior powder particles, to a maximum of 0.5 μm within the bulk of the material (Fig. 8a–e). Fig. 8b and d show, respectively, a 3 μm prior powder particle still retaining its spherical shape containing fine precipitates, and the coarser particles more characteristic of the bulk of the material. Fig. 8c and e show that these second phases are both αAlMnSi. In regions where volume fraction of αAlMnSi was lower, αAl subgrains were evident with size between 300 and 500 nm, usually with the αAlMnSi particles on subgrain boundaries or associated with dislocations. The size distribution of αAlMnSi shown in Fig. 9a and b is consistent with a mean particle diameter of 63 ± 5 nm

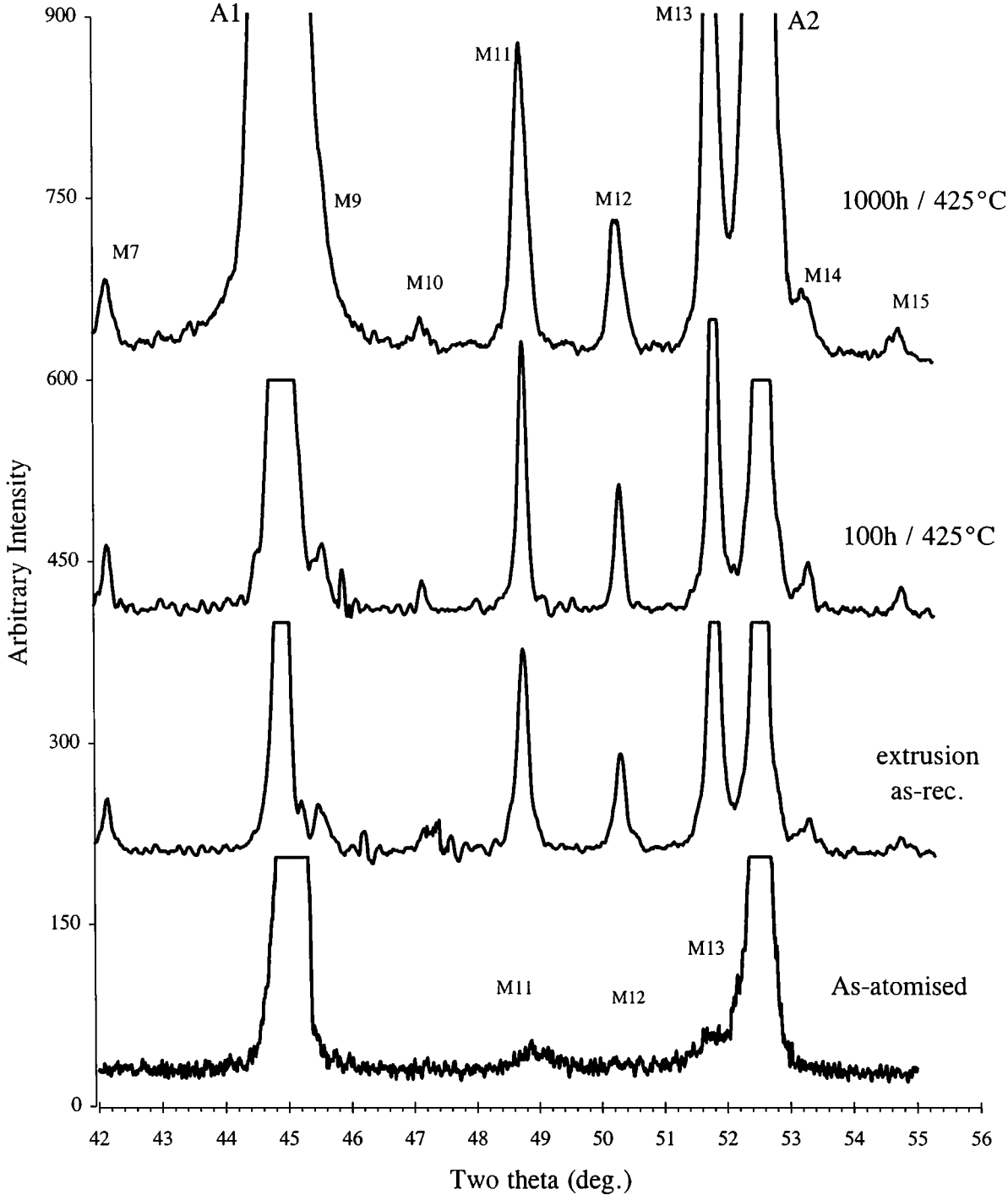

Figure 6 X-ray diffraction traces from as-atomized and as-extruded Al-5 Mn-3 Si powder, showing presence of Al (= A) and αAlMnSi (= M) and the effect of heat treatment of the extruded material at 425 °C.

Peak No	Al	A2	M7	M9	M10	M11	M12	M13	M14	M15
hkl	Al 111	Al 200	α510	α520	α440	α433	α600	α611	α620	α541
*I/I_1	100	40	50	50	10	90	60	100	40	10
†2θ, degrees	45.1	52.5	42.1	45.5	47.0	48.6	58.1	51.6	53.0	54.5

*Powder Diffraction File cards 4-0787 and 6-0669.
†CoKα radiation.

for the as-extruded condition, and is evidently multimodal, peaked at ~50, 100, 230 and 330 nm. Knoop microhardness decreased from 120 ± 11 kg/mm^2 to 89 ± 9 kg/mm^2 as a result of the consolidation conditions employed. Optical microscopy of the extrusion containing 15 vol % SiC (Fig. 10a) showed banding of the SiC particles along the direction of extrusion. SEM (Fig. 10b) showed fine porosity associated with clusters of SiC particles but there was no evidence of a significant reaction zone between SiC and the matrix, which appeared to have been well bonded by the extrusion process. TEM (Fig. 11) confirmed absence of

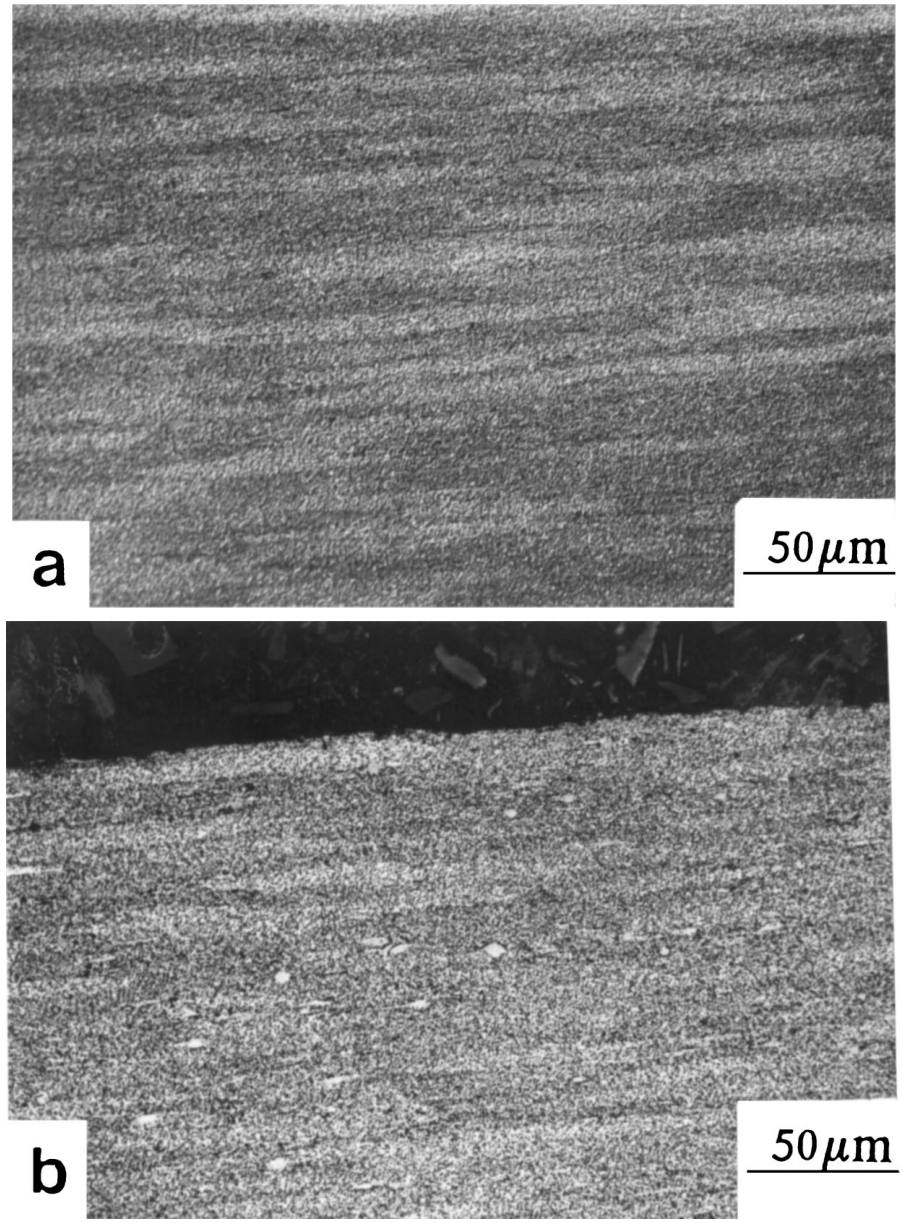

Figure 7 Optical micrographs of longitudinal sections of as-extruded Al-5 Mn-3 Si showing lighter regions and darker regions associated with different microstructural scales within the powder particles. The arrowed Zone A particles in (b) have resisted deformation more effectively than surrounding material.

a reaction zone adjacent to SiC particles with no significant difference in matrix microstructure compared with the SiC-free extrusion.

3.3. Structure of heat treated material

SiC-free extrudate that had been held for 1000 h at 425 °C showed evidence of microstructural coarsening even under the optical microscope. TEM indicated that substantial coarsening had indeed occurred even after 100 h at 425 °C (Fig. 12a) to give an average αAlMnSi particle diameter of 104 ± 8 nm increasing further to 180 ± 14 μm after 1000 h at 425 °C (Fig. 12b) with particles up to 1 μm in size (Fig. 12c). Subgrain size of the matrix had increased to between 500 and 700 nm after 100 h and to between 600 and 1000 nm after 1000 h at 425 °C. XRD showed some increase in intensity of the αAlMnSi peaks but with no significant change in their relative intensities (Fig. 6c, d). Fig. 9a and b show that multimodality in the αAlMnSi size distribution persists on heat treatment with the constituent peaks moving to larger particle sizes with increasing time at 425 °C. Knoop microhardness decreased from 89 ± 9 kg/mm^2 as-extruded to 76 ± 8 and 71 ± 3 kg/mm^2 after 100 and 1000 h at 425 °C.

3.4. Tensile properties of the extruded materials

Table I compares 0.2% proof strength, ultimate tensile strength, Young's modulus and elongation to fracture for as-extruded Al-5 Mn-3 Si with and without reinforcement with 15 vol % SiC and also shows the effects of heat treatment for 100 and 100 h at 425 °C. Results [8, 31] for Allied 8022, 8009 and FVS 1212 (16, 27 and 36 vol % $Al_{13}(Fe, V)_3Si$) are included for comparison. As expected the SiC-reinforced Al-5 Mn-3 Si was stronger and stiffer than the unreinforced material

TABLE I Room temperature tensile mechanical properties of rapidly solidified powder extrusions of Al-5 Mn-3 Si and Al-5 Mn-3 Si/15 vol % SiC as-extruded and after 100 h and 1000 h at 425 °C compared with results [8, 41] for Allied 8022 (Al-6.5 Fe-0.6 V-1.3 Si), 8009 (Al-8.5 Fe-1.3 V-1.7 Si) and FVS1212 (Al-11.7 Fe-1.2 V-2.4 Si) rapidly solidified and extruded. Errors indicated are 95% confidence limits

Material	Treatment	0.2% proof strength, MPa	Ultimate tensile strength, MPa	Young's modulus E, GPa	Elongation to fracture, per cent
Al-5 Mn-3 Si (wt %)	As-extruded	241 ± 5	319 ± 6	84 ± 6	18.3 ± 2.3
	100h/425 °C	182 ± 4	262 ± 4	94 ± 2	18.1 ± 1.6
	1000 h/425 °C	148 ± 9	220 ± 11	96 ± 10	15.9 ± 3.4
Al-5 Mn-3 Si (wt %)	As-extruded	275 ± 0	349 ± 9	112 ± 13	5.9 ± 0.9
plus 15 vol % SiC_p	1000 h/425 °C	229 ± 2	299 ± 2	104 ± 8	4.6 ± 1.0
	1000 h/425 °C	203 ± 2	203 ± 2	125 ± 1	4.1 ± 0.3
8022	As-extruded	260	310	84 ± 1 [41]	22
8009	As-extruded	430	470	88	17
FVS1212	As-extruded	550	590	96	10

but with reduced elongation to fracture. Unreinforced Al-5 Mn-3 Si showed an increase in modulus and a progressive decrease in strength with increase in time of heat treatment. This reduction in strength was proportionately less for the reinforced material. Tensile properties as extruded are very similar to Allied's 8022 alloy which has a similar volume fraction of silicide to Al-5 Mn-3 Si.

4. Discussion

4.1. Microstructure as-atomized and after extrusion

The range of microstructure from segregation-free single phase αAl to two-phase microcellular αAl + αAlMnSi with increase in atomized powder particle size from below a few μm to $\sim$50 μm is typical of Al-transition metal based alloy atomized powders e.g.

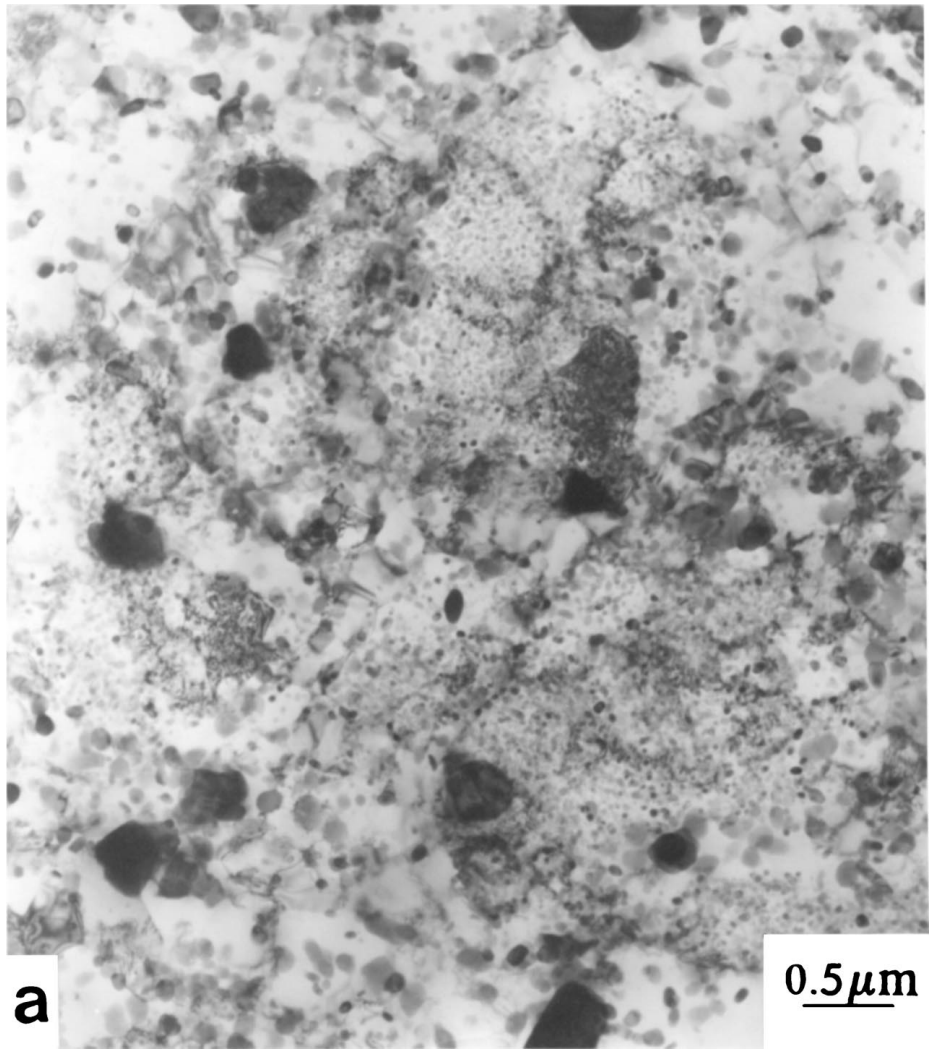

Figure 8 TEM micrographs of extruded Al-5 Mn-3 Si: (a) general microstructure (b) prior powder particle with fine precipitates (c) SAD of precipitates near [1 $\bar{1}$ 1] αAlMnSi (d) more typical second phase scale and distribution (e) SAD of second phase near [0 1 1] αAlMnSi. (*Continued*).

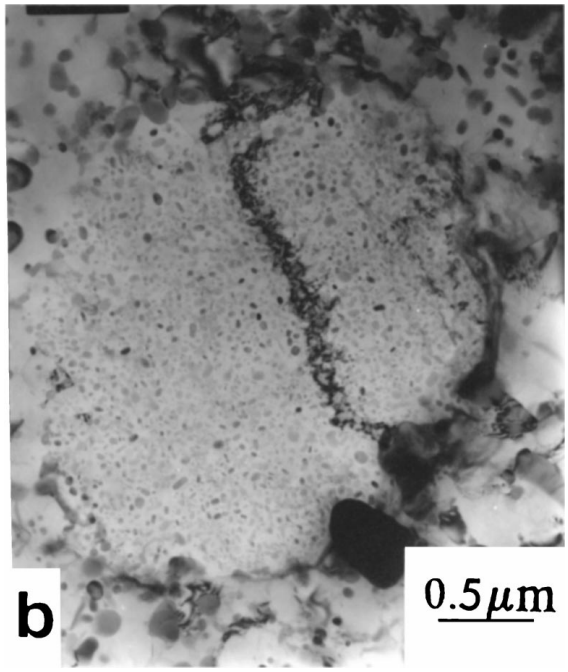

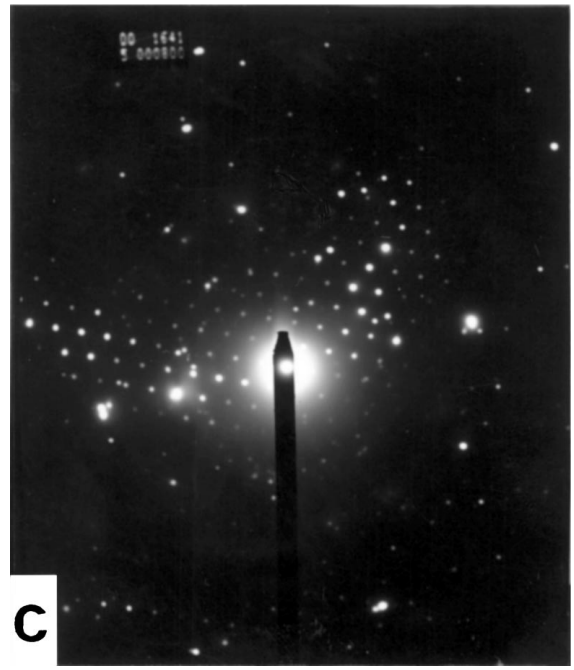

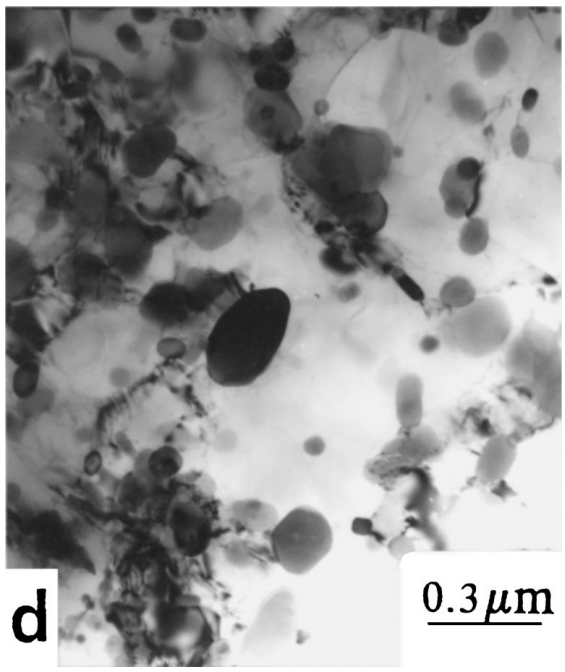

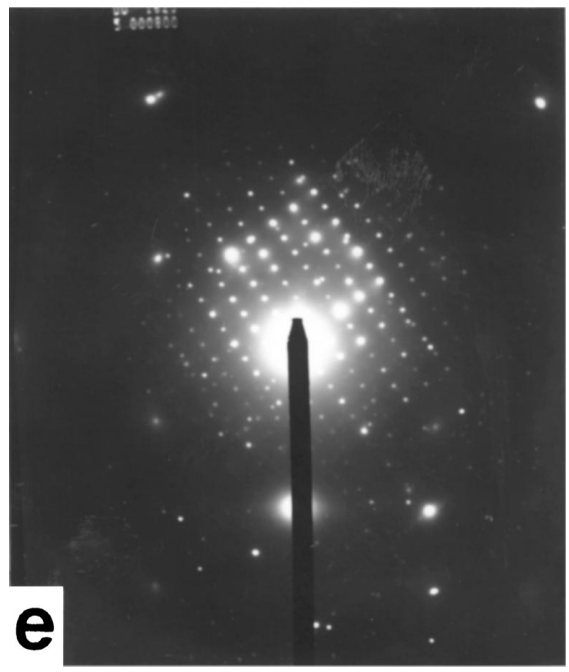

Figure 8 (*Continued*).

[32–39]. The presence of αAlMnSi as the second phase is fully consistent with our observations [25] for melt-spun ribbon of similar composition, which also showed mainly microcellular αAl with intercellular αAlMnSi. The effect of an extended degassing treatment at 425 °C followed by extrusion at 400 °C was to spheroidize the intercellular network to give a multimodal size distribution of αAlMnSi with mean diameter ~60 nm, very comparable with the mean diameter of αAlMnSi particles in melt-spun ribbon of similar composition after 2 to 5 h at 425 °C [26]. The lack of an extensive reaction zone between SiC particles and the matrix in the reinforced sample is also in accord with previous experience for Al-Fe based SiC-reinforced powders extruded under similar conditions [38–40].

4.2. Evolution of microstructure on prolonged heat treatment at 425 °C

The increase in mean αAlMnSi particle diameter from 63 ± 5 nm as-extruded to 104 ± 8 and 180 ± 8 nm after 100 and 1000 h at 425 °C compares with 94 ± 2 and 170 ± 6 nm for melt-spun Al-6 Mn-3 Si after the same heat treatments [26]. Fig. 13 compares the cube of mean particle radius versus time at 425 °C for the two conditions and materials and gives indistinguishable values of slope K 1.7 ± 0.4 and $1.4 \pm 0.6 \times 10^{-28}$ m^2/s and intercept $r_o^3 = 1.3 \pm 0.2$ and $1.1 \pm 0.4 \times 10^{-22}$ m^3, for the extruded and melt-spun samples respectively. The previous paper [26] showed that this $K = 1.7 \times 10^{-28}$ m^3/s is a factor of 5 larger than predictions based on the assumption that volume diffusion of Mn in the αAl

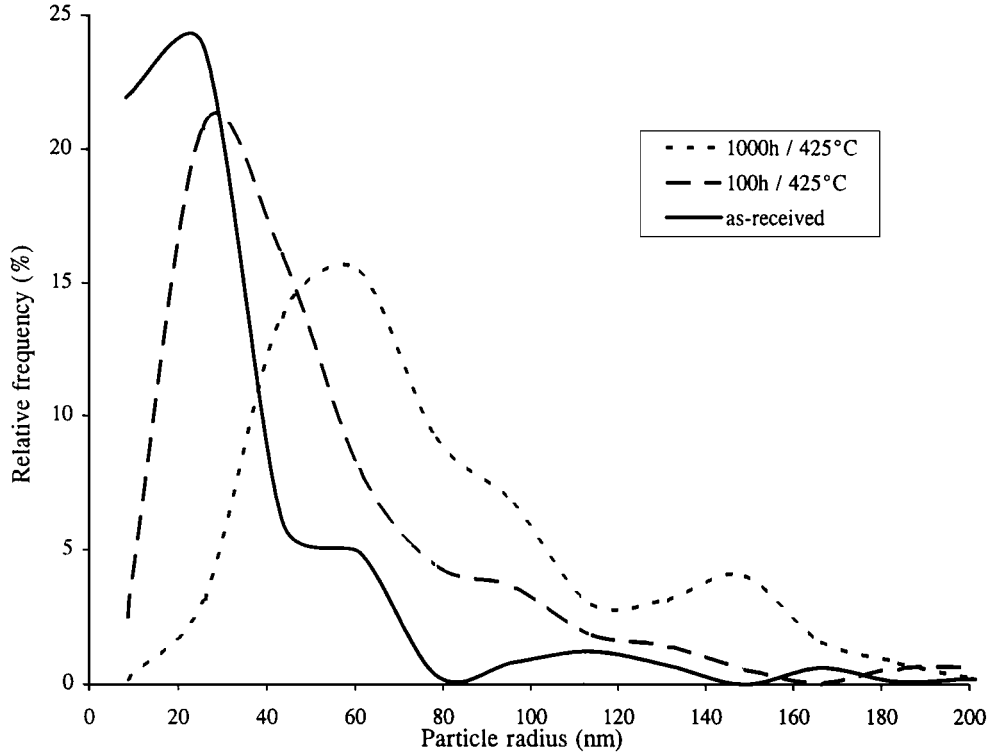

(a)

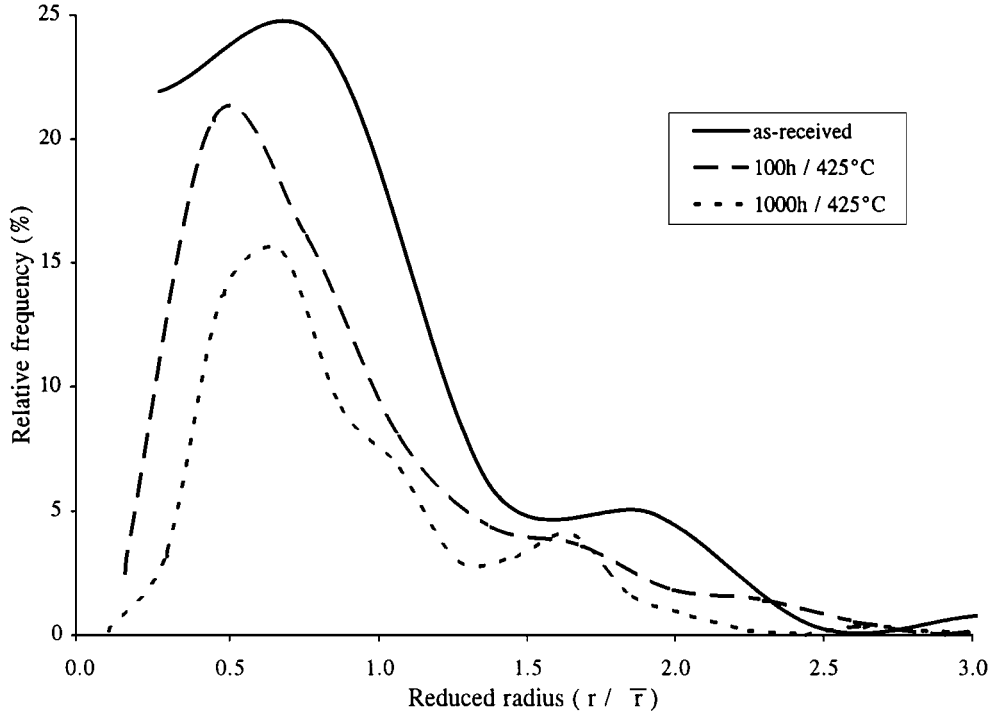

(b)

Figure 9 Size distribution of αAlMnSi in as-extruded and heat treated Al-5 Mn-3 Si against (a) particle radius (b) reduced radius ($r/\bar{r}$).

matrix governs the rate of coarsening of αAlMnSi. The increased observed value was attributed to faster coarsening of αAlMnSi situated on grain boundaries, which was very evident for melt-spun Al-6 Mn-3 Si. A similar enhancement in K could be expected for the extruded Al-5 Mn-3 Si, not least because of subgrains and dislocations derived from the extrusion process. Reasons for the significantly lower coarsening rate of $Al_{13}(Fe, V)_3Si$ in Al-Fe-V-Si alloys of comparable initial particle size are discussed in [25].

4.3. Effects of SiC and particle coarsening on mechanical properties

Extrusion of the Al-5 Mn-3 Si powder at 400 °C gave a material with hardness 90 kg/mm^2, 0.2% proof strength 240 MPa, ultimate tensile strength (UTS) 320 MPa, Young's modulus 84 GPa and elongation to fracture 18%, very similar to Allied's 8022 alloy consolidated from melt-spun ribbon with a similar volume fraction of silicide dispersoid. The earlier paper [26] showed that the hardness of melt-spun Al-6 Mn-3 Si after 1000 h

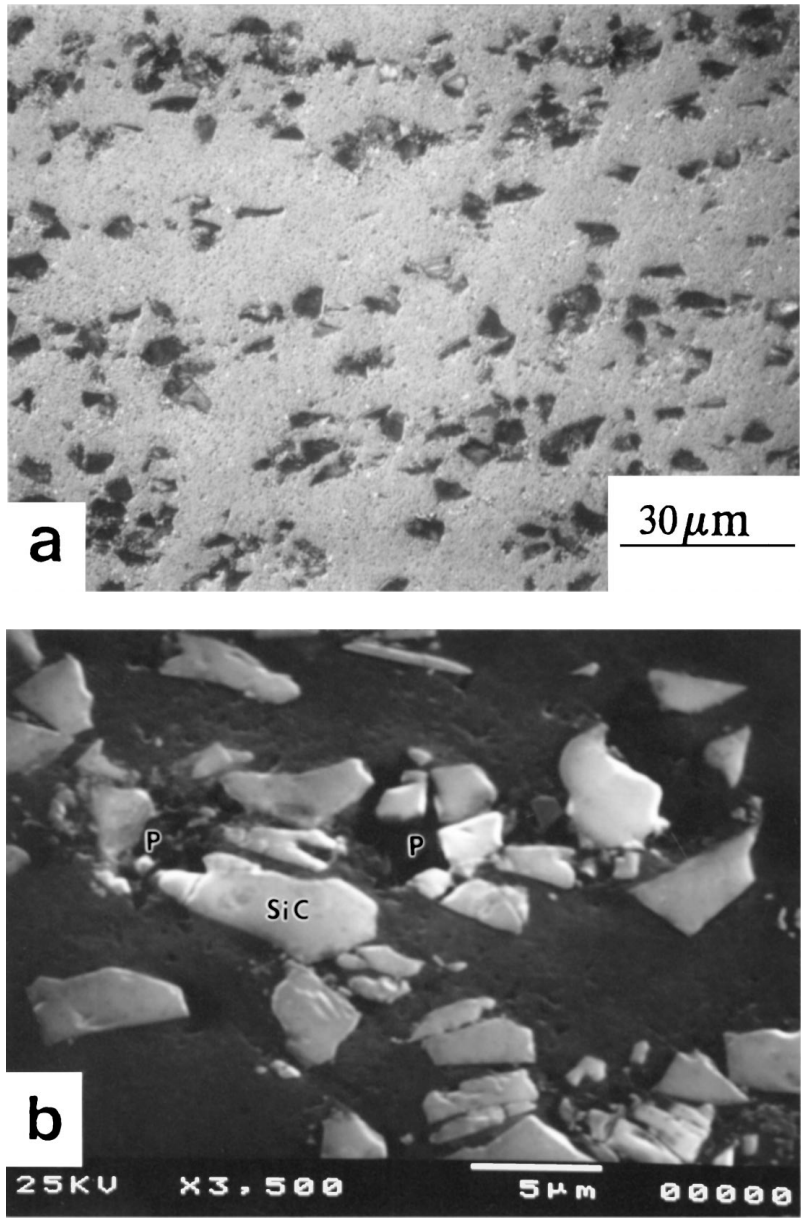

Figure 10 Optical (a) and SEM (b) micrographs showing distribution of SiC particles in Al-5 Mn-3 Si/15 vol % SiC extrusion. P indicates porosity associated with SiC clusters.

at 425 °C could be accounted for by a combination of Orowan hardening from the αAlMnSi dispersoid and a Hall-Petch contribution from the sub-grain size of the αAl matrix. Using the same approach predicts a contribution of 70 kg/mm^2 from Orowan hardening and 30 kg/mm^2 from Hall-Petch, totaling 100 kg/mm^2, similar to the measured value of 90 kg/mm^2. The equivalent predicted yield stress HK/3 is 330 MPa, similar to the measured UTS but overestimating the measured proof strength by some 40 per cent. It is notable, however, that the Orowan contribution drops by some 40% if allowance is made for the fact that the αAlMnSi exhibits a particle size distribution rather than being uniformly sized spheres of radius r. The combined Orowan/Hall-Petch model then also accounts reasonably well for the reduction in hardness and strength on heat treatment. The Orowan contribution is basically inversely proportional to r, and r doubles in 100 h and trebles in 1000 h. The Orowan contribution of 140 MPa to the measured proof strength of 240 MPa thus reduces to 70 and 50 MPa in 100 and 1000 h at 425 °C. Correspondingly the Hall-Petch matrix subgrain size (Λ) contribution is inversely proportional to $\Lambda^{-1/2}$, and Λ increases by factors 1.5 and 2 in 100 and 1000 h at 425 °C. The Hall-Petch contribution of 100 MPa to measured proof strength thus decreases to 80 and 70 MPa in 100 and 1000 h at 425 °C. The combined contributions thus give 150 and 120 MPa after 100 and 1000 h at 425 °C, comparable with the measured values 180 and 150 MPa. The Young's Modulus of 84 GPa as-extruded is virtually identical with the value for Allied's Al-Fe-V-Si with the same volume fraction of silicide [41], consistent with a value of E for the silicide of 150 GPa. The apparent small ($\sim$10%) increase in E after 100 or 1000 h at 425 °C is not readily explained, and may not be significant.

The increment of $\sim$30 MPa in proof and ultimate strengths for the as-extruded MMC in Table I is smaller

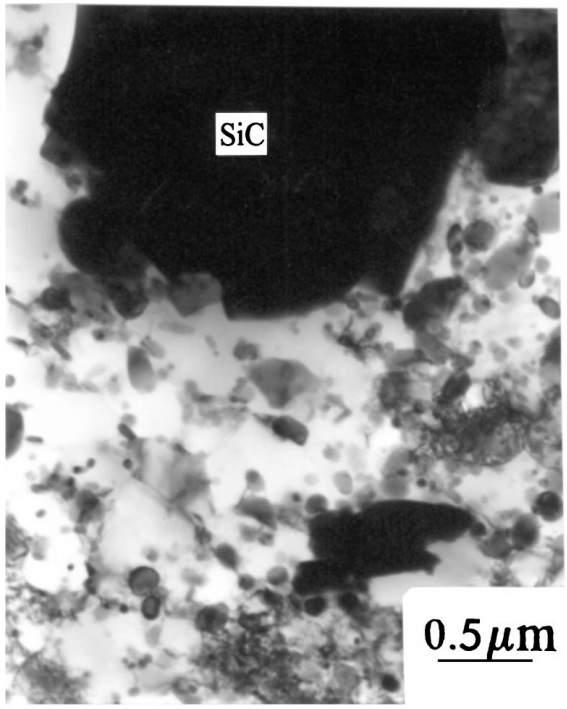

Figure 11 TEM micrograph of extruded Al-5 Mn-3 Si/15 vol % SiC showing absence of a reaction zone adjacent to an SiC particle and matrix microstructure similar to that in the absence of SiC.

than the ~150 MPa increase reported [42] as-extruded 8009 + 15 vol % SiC but the reduction in elongation to fracture from ~18 to ~6 per cent is less than for 8009/SiC (17 to 3 per cent). The reductions in strengths of Al-Mn-Si/SiC in Table I on treatment for 100 and 1000 h at 425 °C are proportionately less, however, than for the unreinforced Al-Mn-Si. The increment in E of ~30 GPa arising from the 15 vol % SiC in the MMC

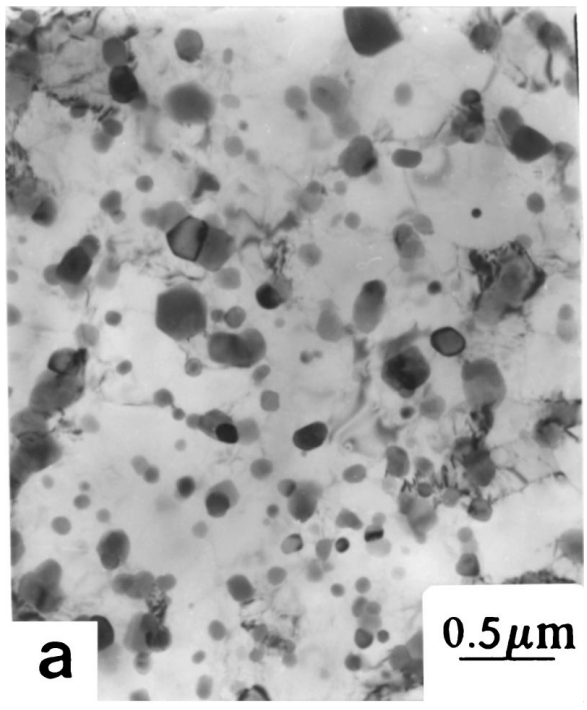

Figure 12 TEM micrograph of extruded Al-5 Mn-3 Si after (a) 100 h and (b, c) 1000 h at 425 °C.

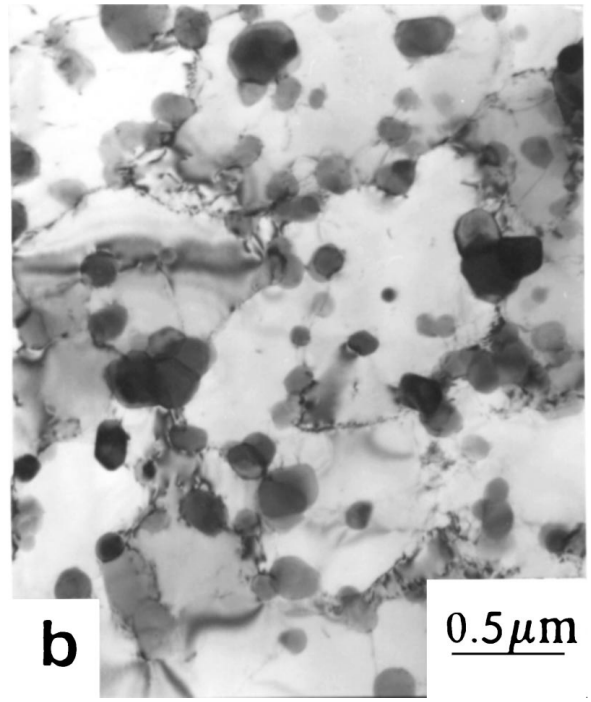

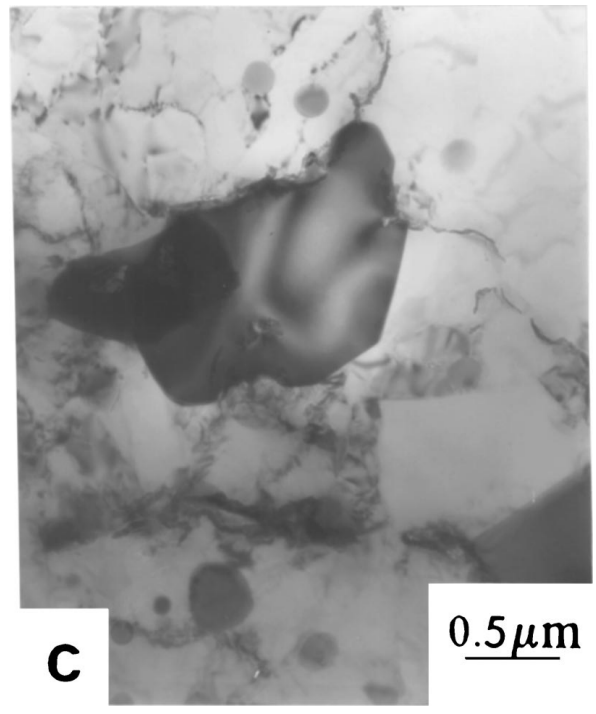

Figure 12 (*Continued*).

is comparable with that obtained for 8009 containing 15 vol % SiC, and is consistent with Reuss averaging of the matrix and SiC moduli with an E for SiC of 97 GPa [43]. The apparent increase in E for the unreinforced material after treatment at 425 °C is less evident for the MMC in Table I.

Finally, Fig. 14 shows measured proof strength versus time of prior treatment at 425 °C for unreinforced material compared with predictions from Orowan and Hall-Petch strengthening and from HV/3. The trend of the measurements aligns with the predictions, and quantitative agreement between them is good for the combined Orowan/Hall-Petch modeling.

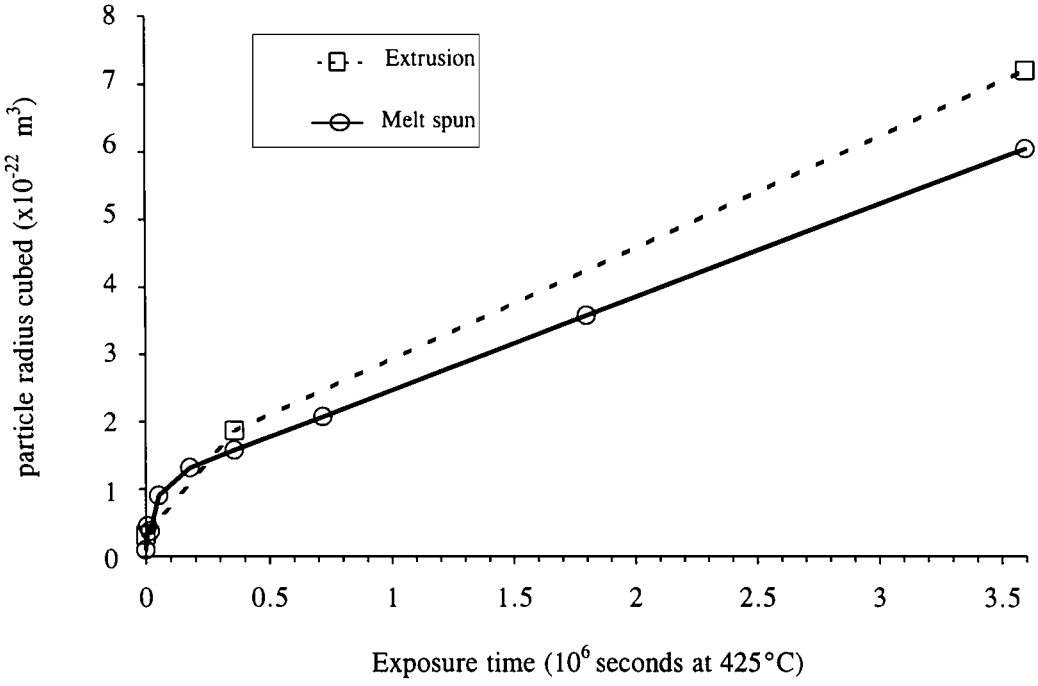

Figure 13 Cube of mean αAlMnSi particle radius versus time at 425 °C for extruded Al-5 Mn-3 Si (present work) compared with melt-spun Al-6 Mn-3 Si [24].

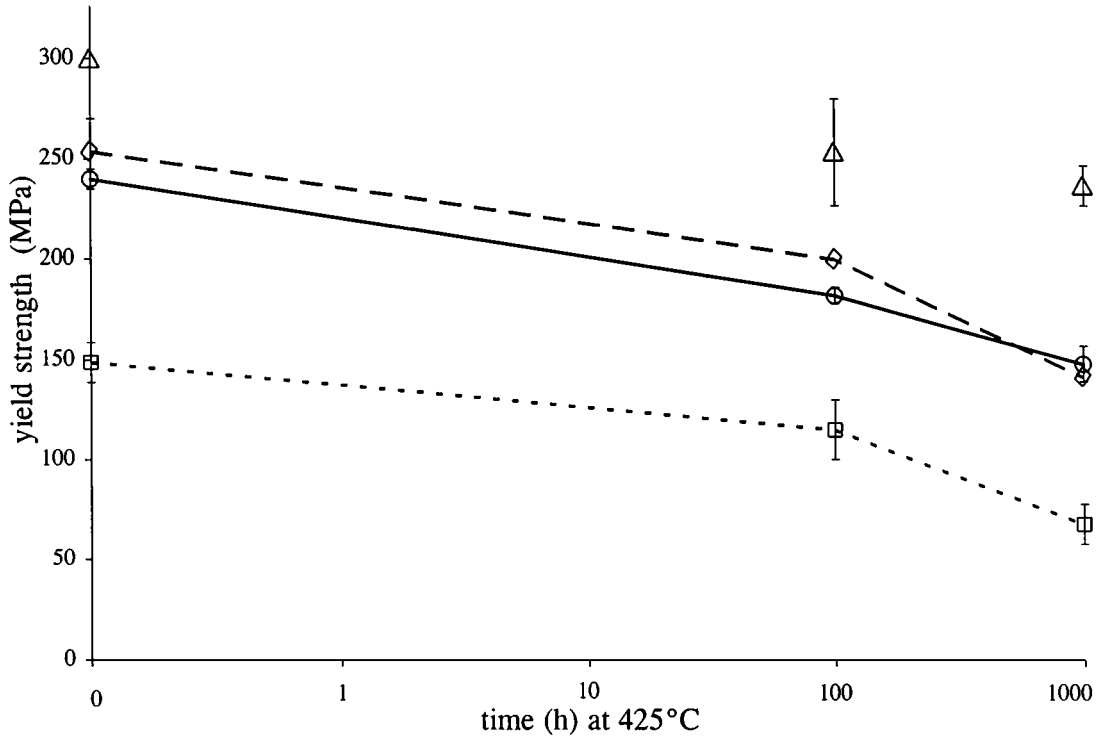

Figure 14 Proof strength versus time of prior treatment at 425 °C for extruded Al-5 Mn-3 Si compared with predictions. Key: ○ measurements, Δ predicted from HV/3, ◊ predicted from combined Orowan and Hall-Petch modelling, □ predicted from Orowan modelling.

5. Conclusions

1. Atomized Al-5 Mn-3 Si powder showed mainly αAl cellular microstructures similar to melt-spun ribbon with intercellular αAlMnSi as the second phase where identification was possible.

2. Consolidation by extrusion at 400 °C with prior vacuum degassing at 425 °C spheroidized the intercellular αAlMnSi to give a microstructure very comparable with that of melt-spun ribbon of similar composition heat treated for 2 to 5 h at 425 °C.

3. The as-extruded microstructure exhibited banding and undeformed 'zone A' particles reflecting the range of microstructures in the as-received powder.

4. Blended-in SiC particulate also exhibited banding but appeared to be well-bonded to the alloy matrix with no signs of a significant interaction zone.

5. Heat treatment at 425 °C produced coarsening of the size distribution of αAlMnSi from an initial mean diameter of 60 nm to 180 nm in 1000 h, very similar to the results for melt-spun ribbon given the same

treatment, while subgrain size of the matrix increased from ~400 to ~800 nm.

6. Levels of hardness and proof strength in extruded Al-5Mn-3Si and their reductions on treatment for 100 and 1000 h at 425 °C can be accounted for by a combination of Orowan and Hall-Petch strengthening as was the case for the hardness of melt-spun material.

7. The increment of ~30 GPa in Young's modulus resulting when 15 vol % SiC was present is similar to that obtained for comparable Al-Fe-V-Si containing 15 vol % SiC, but the associated increments in strength and reductions in elongation to fracture were smaller for the Al-Mn-Si MMC.

Acknowledgement

This work was carried out at the University of Sheffield with support of DERA (Farnborough) under agreement 2031/145/RAE(F).

References

1. M. V. HYATT and S. E. AXTER, in "RASELM 91," ed. K. Hirano et al. (Jap Inst of Light Metals, Tokyo, 1991), pp 273–280.
2. W. WEI, *Metals and Materials* **8** (1992) 430.
3. Y. BARBAUX and G. PONS, *J. Physique IV*, Colloque C7, Supplement III, **3** (1993), 191.
4. J. ZHOU, A. DRUZDZEL and J. DUSZCZYK, *Proc P/M94* **3** (1994) 1587.
5. T. KOIKE and H. YAMAGATA, *ibid*., *idem*. 1627.
6. C. J. PEEL, in "Light Weight Alloys for Aerospace Applications," eds. E. W. Lee et al; (TMS, Warrendale, PA, 1995) pp. 191–205.
7. A. J. SHAKESHEFF and P. D. PITCHER, *Mater Sci. Forum*, **217–222** (1996) 1133.
8. P. GILMAN, *Metals and Materials* **6**(8) (1990) 504.
9. R. E. FRANK and J. A. HAWK, *Scripta Met*, **23** (1989) 113.
10. H. G. PARIS, F. R. BILLMAN, W. S. CEBULAK and J. I. PETIT, in "Rapid Solidification Processing: Principles and Technologies II," eds. R. Mehrabian et al. (Claitor's, Baton Rouge, LA, 1980), pp. 331–341.
11. H. G. PARIS, J. W. MULLINS and T. H. SANDERS JR, in "High Strength P/M Al Alloys," eds. M. J. Koczak and G. J. Hildeman (The Met. Soc AIME, New York, 1982) pp. 277–296.
12. G. TERLINDE, G. LÜTJERING, M. PETERS, J. C. WILLIAMS and H. PARIS, in "High Strength Materials in Aircraft," eds. W. Bunk and J. Hansen (D G M, Oberursel, 1982) pp. 95–112.
13. T. AHRENS, A. GYSLER and G. LÜTJERING, *Z. Metallkunde* **76** (1985) 391.
14. G. TERLINDE, M. PETERS, G. LÜTJERING and J. C. WILLIAMS, *Z. Metallkunde*, **78** (1987) 607.
15. B. SAAL, J. ALBRECHT, G. LUTJERING, J. BECKER and G. FISCHER, in "Light Weight Alloys for Aerospace Applications," eds. E. W. Lee et al. (TMS, Warrendale, PA, 1989), pp. 3–13.
16. B. SAAL, J. ALBRECHT, G. LÜTJERING, J. BECKER and G. FISCHER, in "Advanced Aluminium and Magnesium Alloys," eds. T. Khan and G. Effenberg (ASM, 1990), pp. 299–306.
17. G. LUTJERING, B. SOPART and J. ALBRECHT, in "Science and Engineering of Light Metals," eds. K. Hirano et al. (Jap Inst Light Metals, Tokyo, 1991), pp. 27–34.
18. O. RODER, J. ALBRECHT and G. LÜTJERING, *Proc Euromat 94*, eds. B. Vorsatz and E. Szoke, Vol II, pp. 641–652.
19. O. RODER, J. ALBRECHT and G. LÜTJERING, *Proc ICAA4*, 1994, eds. T. H. Sanders Jr and E. A. Starke Jr, Vol II, pp. 766–773.
20. J. A. HAWKE, L. M. ANGERS and H. G. F. WILSDORF, in "Dispersion Strengthened Aluminium Alloys," eds. Y. W. Kim and W. M. Griffiths (TMS, Warrendale, PA, 1988), pp. 337–354.
21. H. G. F. WILSDORF, L. M. ANGERS, J. K. BRIGGS and J. A. HAWK, in "Advances in P/M," MPIF/APM I, 1989, Vol. 3, pp. 269–283.
22. J. A. HAWK, J. K. BRIGGS and H. G. F. WILSDROF, *ibid.* pp. 301–315.
23. H. G. F. WILSORF, J. K. BRIGGS and L. M. ANGERS, *Key Eng. Mater*., **38, 39** (1989) 318 (Proc ICMS-89, Jamshedpur).
24. E. H. BÜCHLER, E. WATANABE and N. S. KAZAMA, *Internat. J. Non-equilibrium Processing* **10** (1997) 35.
25. D. M. J. WILKES, H. JONES and R. W. GARDINER, *Mater. Sci. Forum* **217–222** (1996) 943.
26. D. M. J. WILKES and H. JONES, *J. Mater. Sci.* **34** (1999) 735.
27. R. HAMBLETON, H. JONES and W. M. RAINFORTH, *Mater. Sci. Eng. A* **A226/8** (1997) 157.
28. H. JONES, *Mater. Sci. Eng.* **5** (1969) 1.
29. C. G. LEVI and R. MEHRABIAN, *Met. Trans. A* **13A** (1982) 13.
30. W. J. BOETTINGER, L. BENDERSKY and J. G. EARLY, *Met. Trans. A* **17A** (1986) 781.
31. P. S. GILMAN and S. K. DAS, *Metal Powder Report* **44** (1989) 617.
32. G. J. MARSHALL, *J. Mater. Sci.* **22** (1987) 3581.
33. M. A. ZAIDI, *Mater. Sci. Eng.* **98** (1988) 221.
34. N. J. E. ADKINS and P. TSAKIROPOULOS, *Mater. Sci. Technol.* **I** (1991) 334.
35. J. ZHON, J. DUSZCZYK and B. M. KOREVAAR, *J. Mater. Sci.* **26** (1991) 3292.
36. G. SHAO, P. TSAKIROPOULOS and A. P. MIODOWNIK, *Internat. J. Rapid Solidification* **8** (1993) 41.
37. M. LIEBLICH, G. CARUANA, M. TORRALBA and H. JONES, *Mater. Sci. Technol.* **12** (1996) 25.
38. V. RADMILOVIC, G. THOMAS and S. K. DAS, *Mater. Sci. Eng. A* **A132** (1991) 171.
39. Z. Y. MO, N. G. NING, Y. X. LU, J. H. LI, J. BI and Y. Z. ZHANG, *Mater. Lett.* **21** (1994) 69.
40. T. J. LIENERT, W. A. BAESLACK III, J. RINGNALDA and H. L. FRASER, *J. Mater. Sci.* **31** (1996) 2149.
41. D. J. SKINNER, in "Dispersion Strengthened Aluminium Alloys," eds. Y. W. Kim and W. M. Griffith (TMS, Warrendale, PA, 1988), pp. 181–197.
42. M. S. ZEDALIS, J. M. PELTIER and P. S. GILMAN, in "Light Weight Alloys for Aerospace Applications," ed. E. W. Lee, E. H. Chia and N. J. Kim (TMS, Warrendale, PA, 1989), pp. 323–334.
43. M. S. ZEDALIS and D. J. SKINNER, in "Light Weight Alloys for Aerospace Applications," eds. E. W. Lee, E. H. Chia and N. J. Kim (TMS, Warrendale, PA, 1989), pp. 335–344.

Received 1 April
and accepted 12 August 1998